



Converting noise into solitons: optical self-organization through intermodal nonlinearity

H. B. KABAGÖZ,^{1,2} A. ANTIKAINEN,¹ AND S. RAMACHANDRAN^{1,3}

¹Boston University, 8 Saint Mary's St, Boston, MA 02215, USA

²kabagoz@bu.edu

³sidr@bu.edu

Abstract: We experimentally demonstrate a pump-pulse-induced conversion of noise into solitons in multimode optical fibers. The process is based on the recently discovered phenomenon of soliton self-mode conversion, where a pump soliton in a higher-order spatial mode crafts another well-defined soliton, originating purely from noise, in a lower-order mode at a longer wavelength through intermodal Raman scattering. The lack of the need for any seed or cavity feedback demonstrates that soliton self-mode conversion is a fundamentally unavoidable, but nevertheless tailorably useful, self-organizing nonlinear optical effect capable of turning noise into transform limited solitons.

© 2021 Optical Society of America under the terms of the [OSA Open Access Publishing Agreement](#)

1. Introduction

Raman scattering is an inelastic scattering process where the incident photon has a different frequency than that of the scattered photon, and energy is transferred to or from lattice vibrations. Generally, the scattered photon has a lower frequency than the incident photon, and a phonon is created upon scattering. For long optical pulses and in the continuous-wave regime, Raman scattering manifests in the generation of a Stokes pulse at a longer wavelength [1]. Due to dispersion, the Stokes pulse and the pump pulse have different phase and group velocities and hence there is temporal walk-off between them. The walk-off can be circumvented by ultrashort solitons where the pump and Stokes pulses are one and the same, self-phase modulation balances out the effects of anomalous dispersion, and the soliton is kept temporally invariant. For a pulse with a spectrum broad enough to span the Raman gain spectrum of the medium, Raman scattering can take place within the pulse, leading to the well-known effect of soliton self-frequency shift (SSFS) manifesting as a gradual continuous red shift of the whole spectrum of the ultrashort soliton [2].

Cavities and waveguides that support multiple spatial or polarization modes offer yet another way to circumvent temporal walk-off between the pump and Stokes pulses. Intermodal dispersion can balance out chromatic dispersion, and the pump and Stokes pulses can co-propagate if they are in suitably different spatial modes. This co-propagation enables Raman-induced energy transfer between the two pulses in two distinct modes. This has been observed in birefringent fibers with the introduction of cross-polarized pulses that are spectrally separated but still fall within the Raman gain spectrum [3], and in microcavities, where the allowed spectral bands of distinct spatial modes are defined by cavity resonances [4]. An extreme manifestation of this effect, called soliton self-mode conversion (SSMC), was recently discovered [5]. Without seeding light into the two group-velocity-locked states or without selectivity such as cavity feedback, SSMC crafts a group-velocity-locked pulse even when a (pump) pulse in only one spatial mode is introduced in a highly multimode fiber. This selective nonlinear coupling happens in spite of the multitude of potential nonlinear scattering pathways amongst the approximately 5,000 modes

such fibers support, in contrast to other known nonlinear phenomena in multimode fibers [6]. Even so, SSMC is highly efficient, offering $\sim 100\%$ photon conversion.

This begs the question – is SSMC a mere multimode generalization of SSFS? After all, pulses undergoing SSMC experience SSFS as well, and manufacturing imperfections in multi-mode fibers can induce random linear coupling between modes. Alternatively, is it more fundamental in nature, and not a consequence of random linear coupling, but instead a unique form of nonlinear self-organization where noise becomes a transform-limited soliton? That is, does it represent a case where a noise-initiated scattering mechanism wins over concurrent seeded phenomena such as SSFS? Theoretical simulations, based on the multimode generalized Schrödinger equation [7], suggest the latter [8], and that even quantum shot noise suffices to facilitate SSMC. However, experimentally, it also appears improbable that random linear coupling would not lead to a “seeding” effect that is more prevalent than quantum shot noise.

Here, we present experimental evidence that SSMC is, perhaps counterintuitively, noise-initiated. By employing shot-to-shot coherence characterization techniques commonly used for supercontinua [9], we show that shot-to-shot *coherent* pump pulses yield shot-to-shot *incoherent* solitons in a different spatial mode. The results show that SSMC represents a curious form of optical self-organization in which noise is turned into a well-defined pulse of order and structure – a transform limited soliton. At the same time, the noisy origins of the soliton are still evident in the shot-to-shot incoherence that the soliton inherits from the noise out of which it was born. Crucially, given the right modal group-velocity distributions in a multimode waveguide, SSMC is fundamentally unavoidable, and not predicated by experimentally indeterminate factors such as random linear coupling.

2. Soliton self-mode conversion

Before evaluating the origins and noise properties of the SSMC effect, we begin by reviewing the experimental conditions that spawn it, along with the characteristics of the pulses and spectra produced therein.

Figure 1(a) illustrates the setup leading to SSMC, comprising an ultrashort pulse ($\sim 100\text{-fs}$) pump at 1045 nm (KMLabs: YFi) operating at 10 MHz, which, after spatial sculpting with a spatial light modulator (SLM: Hamamatsu, X10468), excites a corresponding pulse in the desired mode, with high purity [10], in the higher order mode (HOM) fiber. Since SSMC manifests in nonlinear interactions between pure modes that exhibit group-velocity diversity, the HOM fiber should possess two important linear properties: (1) it should allow for the propagation of a multitude of linearly stable modes; and (2) the system must have non-zero modal dispersion. While several fibers exhibit these characteristics, the simplest design – a step index multimode fiber – readily satisfies these conditions for sufficiently high mode orders, as known from prior work on large mode area fibers [11]. Hence, the experimental setup uses 1.25 meters of step index fiber with a 97- μm core and a numerical aperture (NA) of 0.34, as shown in Figs. 1(b), 1(c). The pump pulse was launched in the $\text{LP}_{0,21}$ mode of the fiber, and the corresponding near-field image at the output of the fiber was recorded with the camera at low power, and thus before the onset of nonlinearities. A sharp, high-contrast image with precisely 20 rings and a central spot clearly suggests high mode purity (Fig. 1(d)). Figures 1(e), 1(f) show subsequent mode images during the SSMC experiment, described further below. The dispersion of the pump mode is anomalous at the pump wavelength and hence solitons can be supported.

Figure 2(a) shows the output spectral evolution (in all modes) as the input power of the launched pulse in the $\text{LP}_{0,21}$ mode is varied, measured with the optical spectrum analyzer (OSA: ANDO, AQ6317B; 0.5-nm resolution, High 1 sensitivity setting). Input power and fiber length are not completely analogous parameters; however, cutback measurements yield similar results as changing the input power [5]. Therefore, the spectra of Fig. 2(a) along with autocorrelation measurements of individual spectral components (not shown) as well as their respective mode

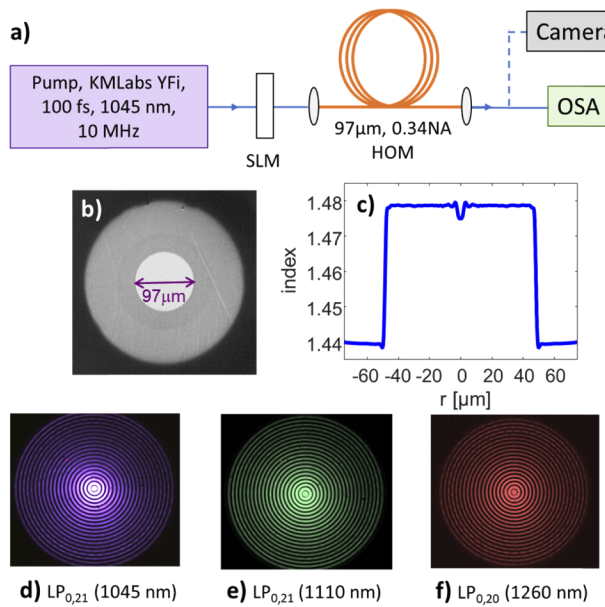


Fig. 1. (a) Experimental setup to probe the behavior of ultrashort pulses in a step index multimode higher order mode fiber. (b) Facet image and the (c) refractive index profile of the fiber (at 1045 nm). (d) Mode image before the onset of nonlinearity ($P_{in} = 10$ mW). (e) Mode image of the SSFS pulse at $P_{in} = 493.7$ mW. (f) Mode image of the SSCM pulse at $P_{in} = 766.7$ mW.

images (shown in Fig. 1(d), 1(e), 1(f)) help discerning the pulse evolution and dynamics. A spectral feature experiencing a continuous spectral shift appears evident up to an input power level, $P_{in} \sim 625$ mW. Time-bandwidth products indicate these are transform-limited pulses. Imaging them reveals that they are in the LP_{0,21} mode; same as the pump mode (Fig. 1(e)). Measuring the pulse energy (25 nJ) and knowing the group-velocity dispersion of this mode at its central wavelength (72.9 ps/nm-km at 1110 nm) helps ascertain that these spectral features are fundamental solitons. Thus, up to $P_{in} \sim 625$ mW, the input pulse appears to have undergone conventional SSFS. At this power level, however, a small spectral feature approximately one Raman Stokes shift away from the SSFS pulse becomes evident. And, as input power is further increased, this feature grows at the expense of the SSFS pulse. Spectrally filtering and imaging the new pulse reveals that it is in the LP_{0,20} mode (exactly one radial mode order lower), as shown in Fig. 1(f). Note that, mid-way through this process, corresponding to $P_{in} \sim 673$ mW, the group indices of the SSFS pulse in the LP_{0,21} mode at 1168 nm and that of this new pulse in the LP_{0,20} mode at 1240 nm are identical. It is this characteristic, of group-velocity matching, that appears to efficiently convert the frequency as well as the spatial mode of light, that is a signature of the SSCM phenomenon.

The distinguishing features of SSCM are as follows: (a) its onset critically depends on group-velocity locking between spectrally separated pulses, and (b) crucially, once it occurs, it strongly and quickly depletes power from an already efficient, seeded (SSFS) process. There are two possibilities for the emergence of the latter characteristic (of a new process, competing with, and subsuming an already existing seeded process, with $\sim 100\%$ photon number efficiency) – SSCM may itself be seeded by random mode coupling arising from environmental perturbations, or it may be a spontaneous, noise-initiated process.

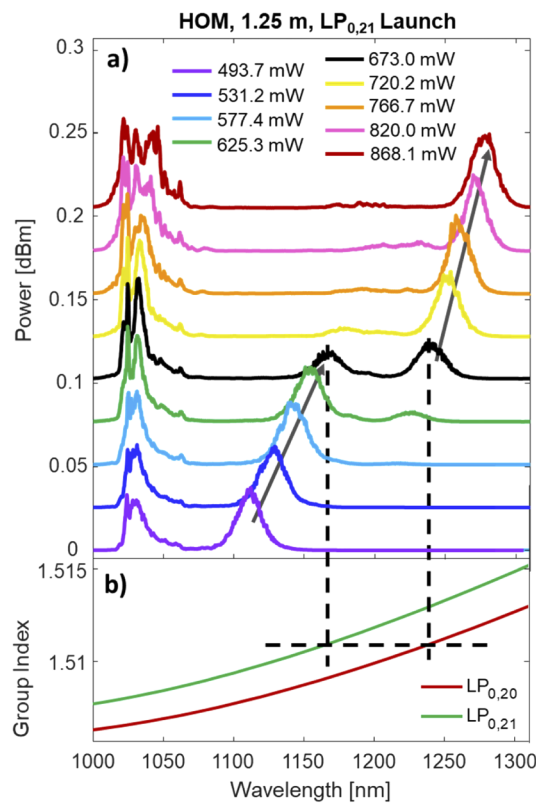


Fig. 2. (a) Measured spectra in all modes with varying input pump power. Pump initially induces conventional SSFS. SSMC onset is evident at 625-mW pump power. Eventually, SSFS pulse completely converts to the new SSMC pulse. (b) Group index vs wavelength for the LP_{0,20} and LP_{0,21} modes.

3. Shot-to-shot coherence measurements

Distinguishing between a seeded and noise-initiated process is possible by studying the shot-to-shot coherence properties of the generated pulse. Seeded processes are expected to inherit the coherence properties of the pump that produced them, whereas noise-initiated phenomena would result in corresponding coherence degradations.

The experimental setup for these measurements, similar to that used for measuring coherence properties of supercontinua [9], is shown in Fig. 3 [12]. The beam, the shot-to-shot coherence of which is to be measured, is split into two with a non-polarizing 50:50 beam splitter, and one arm is delayed by ~ 30 m of free-space propagation, which corresponds to the delay between consecutive pulses. A variable delay in one of the arms (indicated as τ in Fig. 3(f)) allows controlling the relative time delay t_d between consecutive pulse pairs to the sub-picosecond level. Another non-polarizing 50:50 beam splitter recombines the beams, and the combined beam is then collected with a multimode fiber that is connected to an optical spectrum analyzer (OSA: ANDO, AQ6317B) and an autocorrelator (AC: APE, PulseCheck). All spectra presented in this section are measured with 0.04-nm resolution and with the “Mid” sensitivity feature of the OSA. The visibility of the interference fringes, of frequency $\Delta\nu_f = 1/t_d$, reveals the degree of shot-to-shot coherence.

Sufficient care must be exercised to distinguish any degradation of fringe visibility due to the fundamental characteristics we wish to measure from those arising from experimental

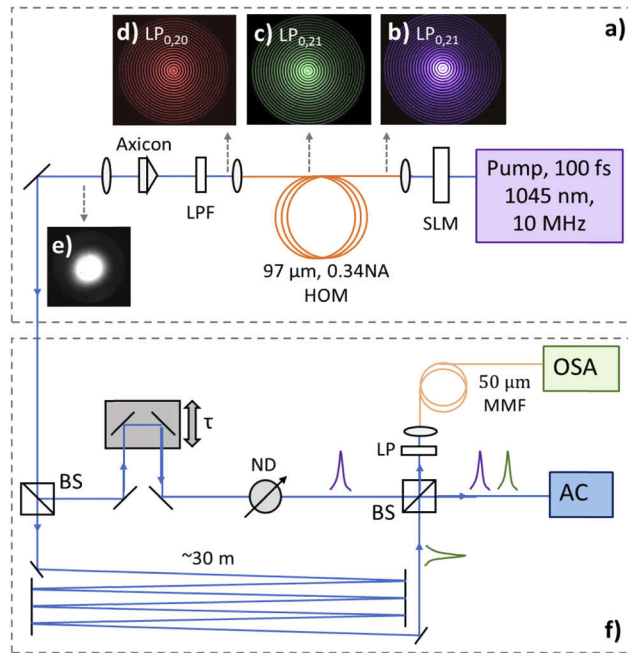


Fig. 3. a) Mode conversion setup. SLM: spatial light modulator, HOM: higher order mode fiber, LPF: long pass filter, BS: beam splitter, τ : variable delay line, ND: variable neutral density filter, LP: linear polarizer, AC: autocorrelator, MMF: multimode fiber, OSA: optical spectrum analyzer. The representative images for the launch mode in the inset (b), the red shifted mode before the soliton self-mode conversion onset in the inset (c) and the mode image after full conversion to the SSMC mode in the inset (d). The reconverted mode image for the SSMC mode in the inset (e). (f) The shot-to-shot coherence measurement setup.

misalignments. Standard precautions include equalizing powers of the two arms with a variable neutral-density (ND) filter, and using a polarizer just before the pickup fiber to ensure interference of only co-polarized beams (see Fig. 3(f)). Relative temporal delays are adjusted such that the fringe spacing on the OSA is small enough to ensure a sufficient number of fringes within the source bandwidth, while keeping it large enough to be spectrally resolvable. The most crucial alignment metric pertains to the fact that, unlike conventional interferometers that measure mixing of Gaussian beams [9], here we measure the interference of two distinct spatial modes. Although an axicon at the output of the HOM fiber converts the Bessel-beam-like LP_{0,20} or LP_{0,21} modes into Gaussian beams [10], this setup is more sensitive to alignment errors. Strict spatial alignment can, however, be sufficiently and confidently assured by measuring auto- and cross-correlation traces. In the time domain, the interferometer results in a dominant auto-correlation peak, and two cross-correlation peaks on either side of the dominant peak, separated by t_d . Ensuring that these cross-correlation peaks are of identical amplitude automatically confirms spatial alignment as any non-collinearity between the two beams will result in uneven spatial overlap of the two beams with each other on different delay positions of the moving arm inside the autocorrelator.

3.1. Pump shot-to-shot coherence

We first establish the baseline shot-to-shot coherence of our pump laser with a power level of 10 mW, with all other specifications (repetition rate, pulse width, etc.) remaining the same. The setup for the measurement is similar to that illustrated in Fig. 3, but with the HOM fiber path, and the axicon that follows it (shown in Fig. 3(a)), replaced by a collimated Gaussian beam path,

since the baseline measurement involves only the pump laser. The pump beam image is shown in Fig. 4(d).

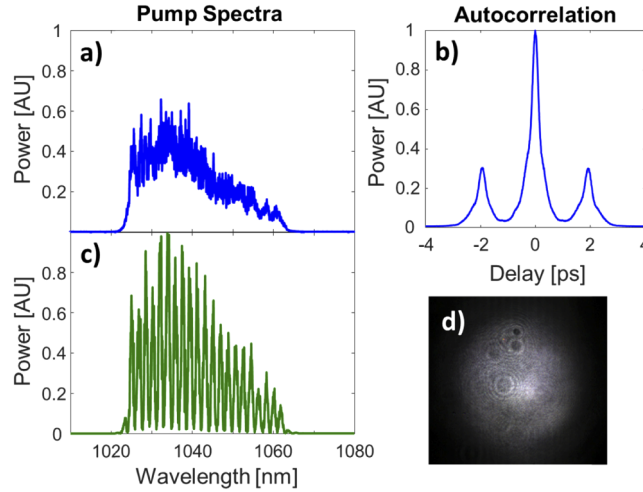


Fig. 4. (a) Pump spectrum with the long arm of the interferometer blocked. (b) Autocorrelation of the pump pulse pairs, equal cross correlation peaks indicate co-aligned beams. (c) Interference spectrum of the pump pulse pairs, fringes show visibility of 95%. (d) Image of the pump beam before the shot-to-shot coherence setup.

Figure 4(a) shows the spectrum recorded on the OSA when the ~30-m arm of the interferometer is blocked, Fig. 4(b) shows the autocorrelation of the recombined beams when they are co-polarized as well as spatially and temporally aligned using the experimental procedures outlined with the discussion of the setup. Equal amplitudes for the cross-correlation peaks of the autocorrelation trace of Fig. 4(b) confirm alignment to ensure maximum fringe visibility. Figure 4(c) shows the interference spectrum recorded on the OSA. Fringe visibility for the interference spectra as a function of wavelength ($V(\lambda)$), which corresponds to the first order mutual spectral coherence in this case, is defined as:

$$V(\lambda) = \frac{I_{\max}(\lambda) - I_{\min}(\lambda)}{I_{\max}(\lambda) + I_{\min}(\lambda)} \quad (1)$$

where I_{\max} is the maximum power and I_{\min} is the minimum intensity of a representative spectral oscillation [9]. Rigorously, the mutual degree of coherence, directly corresponding to fringe visibility, is defined as [13]:

$$|g_{12}(\lambda)| = \left| \frac{\langle E_1^*(\lambda, t) E_2(\lambda, t + t_d) \rangle}{\sqrt{[\langle |E_1(\lambda, t)|^2 \rangle \langle |E_2(\lambda, t + t_d)|^2 \rangle]}} \right| \quad (2)$$

where the angle brackets denote averages over an ensemble, and the subscripts 1 and 2 refer to two different, independently generated pulses. As is evident from Fig. 4(c), calculating visibility simply by using Eq. (1) may result in ambiguities arising from the irregular spectral shapes of the pulses. Hence, across this pump and all subsequent pulses whose visibility we calculate, we employ a Fourier analysis method that normalizes for the spectral shape, uses the same super-Gaussian spectral windowing function $g(\omega)$ of order 2.75, and analyzes the resultant Fourier spectra across the same relative temporal bandwidths. The mathematical expressions

that describe the visibility (V) calculated with this method are given in Eqs. (3) to (5) as follows:

$$V = \frac{2 \int_{t_d - \Delta\tau/2}^{t_d + \Delta\tau/2} J(t) dt}{\int_{0 - \Delta\tau/2}^{0 + \Delta\tau/2} J(t) dt} \quad (3)$$

$$J(t) = F^{-1}\{S_I(\omega) \times g(\omega)\} \quad (4)$$

$$g(\omega) = e^{-\left(\frac{(\omega - \omega_0)^2}{2\omega_A^2}\right)^{2.75}} \quad (5)$$

where ω_0 is the central frequency and ω_A is the spectral bandwidth of the super-Gaussian windowing function, $S_I(\omega)$ is the normalized interference spectrum, and $\Delta\tau$ is the temporal integration bandwidth. For this pump laser, we calculate a fringe visibility $V \sim 95\%$, indicating almost perfect shot-to-shot coherence, as would be expected from a low relative intensity noise (RIN) mode-locked oscillator (manufacturer-specified root mean square power fluctuation $< 1\%$).

3.2. SSFS shot-to-shot coherence

Next, we measure the shot-to-shot coherence of the SSFS pulse – i.e. the pulse that is carved out of the pump, resulting in a conventional SSFS-based soliton pulse. Recalling the spectra of Fig. 2, SSFS pulses are obtained when $P_{in} < 625.3$ mW. With $P_{in} \sim 493.7$ mW, an SSFS soliton with ~ 25 -nJ pulse energy at 1110 nm is obtained, as seen in the spectrum of Fig. 5(a), recorded by blocking the ~ 30 -m arm shown in Fig. 3(f). The corresponding image of this soliton is shown in Fig. 5(d). Autocorrelation traces with equal amplitudes for the cross-correlation peaks assure collinearity and spatial overlap, as shown in Fig. 5(b). The interference spectrum obtained with both arms of the interferometer unblocked is shown in Fig. 5(c).

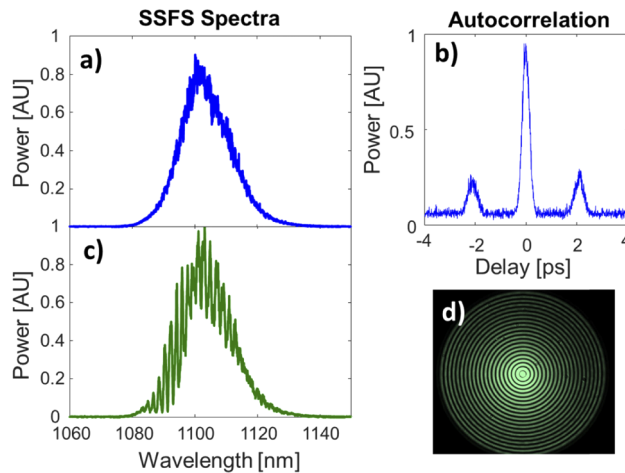


Fig. 5. (a) SSFS spectrum with long arm of the interferometer blocked, SSFS soliton spectrally filtered. (b) Autocorrelation of the SSFS pulse pairs, confirming spatial beam alignment. (c) Interference spectrum of the SSFS pulse pairs, fringes show maximum visibility of 64% on the blue side. (d) Image of the SSFS beam before the reconversion to Gaussian with axicon.

Employing the Fourier analysis method mentioned earlier, we calculate the fringe visibility for the whole of the SSFS spectrum to be 34%. However, the SSFS interference spectrum in Fig. 5(c) shows uneven fringe visibility between the blue and red spectral portions of the soliton, respectively. This is a known and expected effect as a result of the transfer of the pump RIN to

fluctuations in the SSFS soliton wavelength [14], and serves to degrade its coherence for longer spectral shifts [15]. To accurately analyze the uneven fringe visibility of the SSFS spectra, we separate the SSFS spectra into two bins by using the super-Gaussian function of the same order but half the bandwidth ($\omega_A/2$) as the function we used to calculate the visibility of the whole of the SSFS spectra (single bin case). The resultant visibility (V) of the blue portion of the SSFS spectrum is $\sim 64\%$ and that of the red portion is $\sim 15\%$. As expected, the self-seeded SSFS process retains a high degree of coherence of the original pump pulse, especially on the bluer spectral portion.

3.3. SSMC shot-to-shot coherence

As shown in Fig. 2, the SSMC process is completed, and a purely SSMC-driven soliton survives, when $P_{in} \sim 766.7$ mW. We use this soliton for shot-to-shot coherence measurements. The resultant spectrum is shown in Fig. 6(a), with the ~ 30 -m arm blocked. The mode image of the spectrally filtered SSMC peak in the $LP_{0,20}$ mode, centered around 1260 nm, is shown in Fig. 6(d). The pulse energy of the SSMC pulse is measured to be ~ 26 nJ.

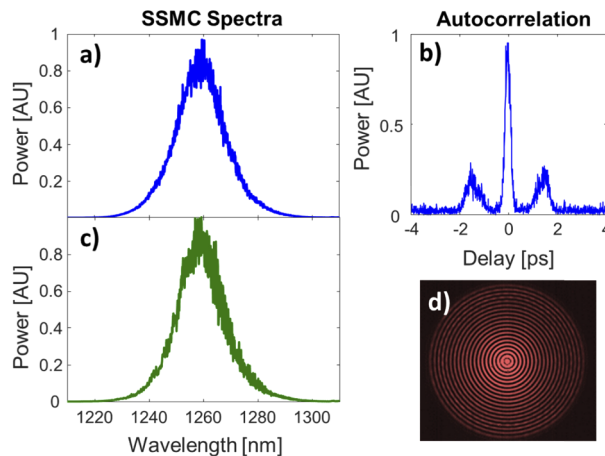


Fig. 6. (a) SSMC spectrum with long arm of the interferometer blocked. SSMC soliton spectrally filtered. (b) Autocorrelation of the SSMC pulse pairs, co-aligned beams. (c) Interference spectrum of the SSMC pulse pairs – no apparent fringes, suggesting complete loss of shot-to-shot coherence. (d) Image of the SSMC beam before the reconversion to Gaussian with axicon.

The autocorrelation trace for the interfered output of the SSMC pulse (Fig. 6(b)) reveals equal amplitudes for the cross-correlation peaks, again, assuring collinearity and spatial overlap. The interference spectrum for SSMC pulses is shown in Fig. 6(c). While no interference fringes are apparent, the visibility, calculated with the single bin Fourier analysis, is 3.6%. An equivalent calculation conducted on two separately recorded pump spectra, each measured with one of the arms blocked (i.e. spectra of the kind shown in Fig. 4(a)) yields $V \sim 3\%$. Since there can be no interference when one of the arms is blocked, this clearly indicates that this is the noise floor for our setup.

Figure 7 is a comparative chart of the visibility of every pulse described above. The visibility shown here represents the worst-case scenario, where it is calculated over the entire bandwidth of a pulse. Note that this underestimates the visibility for SSFS pulses given the distinct behavior of its red and blue spectral portions. Such variations are shown with error bars for each data point.

Hence, while shot-to-shot coherence measurements, as quantified by spectral visibility V , was very high (95%) for the pump pulse and preserved (34% overall visibility with maximum

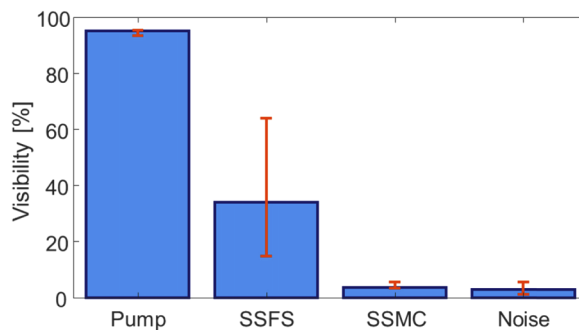


Fig. 7. Visibility for pump, SSFS, SSMC and noise cases. The visibility values shown with the blue bars are from the single bin calculations and the errors bars shown in orange are from the two bin calculations of the visibility.

visibility of 64% on the bluer side) for the nonlinearly sculpted conventional SSFS pulse in this fiber, the visibility of the SSMC-derived soliton is within the error range of the noise floor (1.2-5.6%) of our measurement. From this, we conclude that the SSMC soliton displays no observable shot-to-shot coherence.

4. Discussion, summary and conclusions

Soliton self-mode conversion (SSMC) represents an alternative nonlinear scattering pathway in multimode fibers, which has no single-mode analogue, to the best of our knowledge. It shares attributes with the well-known soliton self-frequency shift (SSFS) process that occurs in single-mode as well as multimode fibers, in that, under favorable conditions, it offers efficient (~100% photon number) conversion and yields frequency-down-converted ultrashort pulses across wide wavelength ranges. Here, we experimentally demonstrate that the newly discovered SSMC process is strictly noise-initiated and does not arise from inadvertent random mode coupling serving to seed the process. This is evident because any seeded nonlinearly crafted pump would retain some of the coherence properties of the pump that enables it, whereas the SSMC pulse is shot-to-shot incoherent even when facilitated by a pump with near unity shot-to-shot coherence.

Hence, SSMC is not just a multimode generalization of SSFS, but in fact, a rather unique manifestation of Raman scattering. It represents optical self-organization through the birth of a soliton purely out of noise, and the process completely depletes power from the parent soliton, which was seeded. As such, SSMC represents a rather counterintuitive case of a robust coupling mechanism capable of turning noise into transform limited pulses and subsuming an already existing seeded process (of conventional SSFS).

This fundamental feature has practical implications for the emerging field of multimode nonlinear optics, which has already provided new degrees of freedom for nonlinear scattering. Many intermodal nonlinear phenomena rely on the interplay of linear and nonlinear mixing [16]. Since linear mixing is strongly a function of the perturbative ambient in which the fiber exists, such nonlinear responses can potentially be sensitive to fiber perturbations. In contrast, SSMC derives from noise and has *no* reliance on the linear properties of the fiber modes (except for the requirement that each mode be individually, linearly stable – a condition readily achieved in step-index fibers). Hence, SSMC, and the energy or wavelengths of pulses it can be tailored to yield [5,17], is impervious to ambient conditions. Likewise, its universality also implies that it should occur not only in step-index fibers, but also in any multimode system, such as on-chip waveguides and coupled-core fibers [18], which offer robust higher order mode propagation with group-velocity diversity.

Funding. National Science Foundation (DGE-1633516, ECCS-1610190); Office of Naval Research (N00014-17-1-2519); Air Force Office of Scientific Research (FA9550-14-1-0165); U.S. Department of Defense Vannevar Bush Faculty Fellowship (N00014-19-1-2632).

Acknowledgments. The authors would like to thank P. S. J. Russell and F. Kärtner for queries that motivated this study, as well as G. P. Agrawal and L. Rishøj for insightful discussions.

Disclosures. The authors declare no conflicts of interest.

Data availability. Data underlying the results presented in this paper are not publicly available at this time but may be obtained from the authors upon reasonable request.

References

1. R. H. Stolen, E. P. Ippen, and A. R. Tynes, "Raman oscillation in glass optical waveguide," *Appl. Phys. Lett.* **20**(2), 62–64 (1972).
2. F. M. Mitschke and L. F. Mollenauer, "Discovery of the soliton self-frequency shift," *Opt. Lett.* **11**(10), 659–661 (1986).
3. N. Nishizawa and T. Goto, "Trapped pulse generation by femtosecond soliton pulse in birefringent optical fibers," *Opt. Express* **10**(5), 256–261 (2002).
4. Q. F. Yang, X. Yi, K. Y. Yang, and K. Vahala, "Stokes solitons in optical microcavities," *Nat. Phys.* **13**(1), 53–57 (2017).
5. L. Rishøj, B. Tai, P. Kristensen, and S. Ramachandran, "Soliton self-mode conversion: revisiting Raman scattering of ultrashort pulses," *Optica* **6**(3), 304 (2019).
6. L. G. Wright, D. N. Christodoulides, and F. W. Wise, "Controllable spatiotemporal nonlinear effects in multimode fibres," *Nat. Photonics* **9**(5), 306–310 (2015).
7. F. Poletti and P. Horak, "Description of ultrashort pulse propagation in multimode optical fibers," *J. Opt. Soc. Am. B* **25**(10), 1645 (2008).
8. A. Antikainen, L. Rishøj, B. Tai, S. Ramachandran, and G. P. Agrawal, "Fate of a soliton in a high order spatial mode of a multimode fiber," *Phys. Rev. Lett.* **122**(2), 023901 (2019).
9. J. W. Nicholson, A. D. Yablon, M. F. Yan, P. Wisk, R. Bise, D. J. Trevor, J. Alonso, T. Stockert, J. Fleming, E. Monberg, F. Dimarcello, and J. Fini, "Coherence of supercontinua generated by ultrashort pulses compressed in optical fibers," *Opt. Lett.* **33**(18), 2038 (2008).
10. J. Demas, L. Rishøj, and S. Ramachandran, "Free-space beam shaping for precise control and conversion of modes in optical fiber," *Opt. Express* **23**(22), 28531 (2015).
11. S. Ramachandran, J. M. Fini, M. Mermelstein, J. W. Nicholson, S. Ghalmi, and M. F. Yan, "Ultra-large effective-area, higher-order mode fibers: a new strategy for high-power lasers," *Laser Photonics Rev.* **2**(6), 429–448 (2008).
12. H. B. Kabagöz, A. Antikainen, and S. Ramachandran, "Experimental Demonstration of the Noisy Origins of Soliton Self-Mode Conversion," CLEO 2020, FTh1.A.
13. J. M. Dudley, G. Genty, and S. Coen, "Supercontinuum generation in photonic crystal fiber," *Rev. Mod. Phys.* **78**(4), 1135–1184 (2006).
14. G. Zhou, M. Xin, F. X. Kärtner, and G. Chang, "Timing jitter of Raman solitons," *Opt. Lett.* **40**(21), 5105 (2015).
15. A. Antikainen, H. B. Kabagöz, and S. Ramachandran, "Fragility of a soliton's shot-to-shot coherence," *Opt. Lett.* **45**(19), 5393 (2020).
16. K. Krupa, A. Tonello, A. Barthélémy, T. Mansuryan, V. Couderc, G. Millot, P. Grelu, D. Modotto, S. A. Babin, and S. Wabnitz, "Multimode nonlinear fiber optics, a spatiotemporal avenue," *APL Photonics* **4**(11), 110901 (2019).
17. H. B. Kabagöz, S. Zhang, L. Rishøj, A. Antikainen, and S. Ramachandran, "Time-Synchronized 3-Color Single-Aperture Fiber Sources via Soliton Self-Mode Conversion," CLEO 2020, SM1P.7.
18. A. Antikainen and G. P. Agrawal, "Soliton supermode transitions and total red shift suppression in multi-core fibers," *Opt. Lett.* **44**(17), 4159 (2019).